Semiconductor Science and Technology

PAPER

Electronic structure, magnetic and optic properties of spinel compound $NiFe_2O_4$

To cite this article: K Bouferrache *et al* 2020 *Semicond. Sci. Technol.* **35** 095013

IOP Publishing Semiconductor Science and Technology
Semicond. Sci. Technol. **35** (2020) 095013 (17pp) https://doi.org/10.1088/1361-6641/ab9845

Electronic structure, magnetic and optic properties of spinel compound $NiFe_2O_4$

K Bouferrache[1], Z Charifi[1,2,6], H Baaziz[1,2], A M Alsaad[3] and Ahmad Telfah[4,5]

[1] Department of Physics, Faculty of Science, University of M'sila, 28000, M'sila, Algeria
[2] Laboratory of Physics and Chemistry of Materials, University of M'sila, M'sila, Algeria
[3] Department of Physical Sciences, Jordan University of Science & Technology, P.O. Box 3030, Irbid 22110, Jordan
[4] Leibniz Institut für Analytische Wissenschaften-ISAS-e.V., Bunsen-Kirchhoff-Straße 11, 44139, Dortmund, Germany
[5] Hamdi Mango Center for Scientific Research (HMCSR), The University of Jordan (UJ), Amman 11942, Jordan

E-mail: charifizoulikha@gmail.com and zoulikha.charifi@univ-msila.dz

Received 3 April 2020, revised 19 May 2020
Accepted for publication 1 June 2020
Published 27 July 2020

Abstract

We report *ab initio* investigation of structural, electronic, magnetic and optical properties of the $NiFe_2O_4$ compound. Hubbard parameters are computed for both *Ni* and *Fe* atoms. Employing generalized gradient approximation (GGA) and GGA + U approximations and taking into consideration four possible types of atomic arrangements, we identify the most stable structural–magnetic configuration of the system. Interestingly, the inverse spinel $NiFe_2O_4$ compound is found to exhibit a ferrimagnetic structure. The ground state structural lattice parameters and the interatomic distances of spinel $NiFe_2O_4$ compound are computed. Furthermore, band structure calculations demonstrate that $NiFe_2O_4$ compound exhibits large band gaps in both spin configurations with a large magnetic moment. Energetically, ferrite nickel favors the inverse spinel phase in which Fe and Ni cations in either octahedral or tetrahedral sites adopt the high-spin configuration. We found that the energy of the normal spinel is higher than that of the inverse spinel, confirming that inverse spinel is the most stable structure of the $NiFe_2O_4$ compound. The optical behavior of the $NiFe_2O_4$ compound is characterized by calculating the real and imaginary part of the dielectric function, the absorption coefficients, the refractive index, the optical conductivity and the energy loss. Optimizing structural, electronic, magnetic and optical properties of this novel compound is crucial for exploring and utilizing it for modern device applications.

Keywords: spinel, Hubbard, ferrites, high spin configuration, magnetic moment, structural, optical properties

(Some figures may appear in colour only in the online journal)

1. Introduction

For the past three decades, advanced functional materials have attracted a great deal of interest. In particular, transition metal oxides have played a critical role in revolutionizing a new generation of advanced devices. At the microscopic scale, the interactions between the transition metals and the oxygen anions are very sensitive to the bonds' length and their angles. Therefore, a diversity of physical, chemical, electronic, magnetic and optical properties within the same structural family is expected.

The spinel oxides are peculiar due to the fact that they can be half-metallic, such as Fe_3O_4, ferrimagnetic insulators like most of the spinel ferrites, transparent conductors such as Cd_2SnO_4 superconductors such as (LTi_2O_4), or heavy fermion compounds like LiV_2O_4. Consequently, they exhibit a variety

[6] Author to whom any correspondence should be addressed.

of physical and electronic properties, enabling them to be potential candidates for modern technological magnetic and optoelectronic devices. They have been employed for a wide range of applications such as catalysts for decomposition of gases [1, 2], high-speed digital tape and disk recording, repulsive suspension for use in levitated systems, catalysis, and magnetic refrigeration systems and magneto-optical storage media [3], flux guides and sensors in thin film recording heads [4], ferromagnetic semiconductors [5], ferro-fluids [6], multiferroic composites [7–10], transformer cores and microwave devices/microwave absorbers and waveguides in the gigahertz region [11] and as magnetic nanoparticles in medical applications [12]. This is due to their high resistivity, low dielectric losses, mechanical hardness, high Curie temperature and chemical stability.

Since the ferrites are stable, easy to prepare and relatively inexpensive, they cannot be replaced by other magnetic materials. They have become technologically attractive. Nickel ferrites adopt a spinel structure in which oxygen atoms form a face-centered cubic lattice (CFC). Each atom is surrounded by divalent and trivalent cations *A* and *B*, respectively. If the structure is of direct type, i.e. the tetrahedral sites (T_d) are occupied by 1/8 of the cations A^{2+}, on the other side the B^{3+} are in half of the octahedral sites (O_h)

The general formula of this compound can be written as $[A_{\mathrm{Td}}{}^{2+}]\ [B_{\mathrm{Oh}}{}^{3+}]_2[O^{2-}]_4$. The inverse spinel structure is generated when cations A^{2+} are replaced by half of B^{3+} cations that has been observed experimentally. The general formula of inverse spinel can be written as $[B_{\mathrm{Td}}{}^{3+}]\ [A_{\mathrm{Oh}}{}^{2+}B_{\mathrm{Oh}}{}^{3+}]\ [O^{2-}]_4$.

Practically, spinel structures are not perfect. Several studies have revealed a migration of cations X^{2+}between sites *A* and *B* [13, 14], leading to 'mixed' spinel structures whose magnetic moments and band structures differ significantly from those of an ideal inverse spinel. Our study is geared towards an investigation of the structural, electronic, magnetic and optical properties of the $NiFe_2O_4$ compound. A pioneering study by Nicolau *et al* [15] shows that $NiFe_2O_4$ has a high Curie temperature and a resistivity of 1kΩ cm at room temperature. Furthermore, Cormack *et al* [16] found that $NiFe_2O_4$ has a low probability of cation inversion, and it acts as a model system in the large group of magnetic insulators in the spinel oxide group.

In order to optimize the structural, magnetic and optical properties of the spinel compound $NiFe_2O_4$, we calculate the Hubbard parameter *U* of both *Ni* and *Fe* atoms in both octahedral and tetrahedral sites in normal and invers phase using the Madsen [16] and Anisimov [17] methods, and identify the stable magnetic phase of the $NiFe_2O_4$ compound. We calculate its electronic behavior by calculating its band structure and the density of the states. In addition, we calculate its total magnetic moment in its ground state. Having calculated the structural and electronic properties, we then focus our attention on calculating its optical properties. The remaining parts of this paper are organized as follows: section 2 contains the details of the calculations. In section 3, we present, analyze and interpret the results and findings of the work. In section 4, we conclude our work.

2. Computational details

Self-consistent *ab initio* calculations using augmented plane wave plus local orbital APW + lo method with total full potential (FP-LAPW) implemented in the Wien2k code are performed [18]. In calculating the structural, magnetic and optical properties, we employed the exchange-correlation potential treated using the generalized gradient approximation (GGA) parameterized by Perdew, Burke and Ernzerhof [19]. The modified Becke–Johnson approach (mBJ) [20] was used to calculate electronic properties. The oxide systems are characterized by a strong electron–electron correlation; therefore, DFT+U approximation [17] is applied. In this approximation, the effects of the on-site Coulomb correlation '*U*' and the Hund coupling '*J*' (in our case $J = 0$ eV) with *U* (eff) = *U*-*J*, are used as proposed by Dudarev *et al* [21]. In order to implement the FP-LAPW approach effectively, we divide the unit cell into two regions, mainly, inside the non-overlapping sphere, we use spherical harmonic expansion to express the charge density and the potentials are expressed via spherical harmonic expansion with angular momentums up to $\mathrm{l_{max}} = 10$. $R_{.M.T}$ radius of *Fe, Ni*, and *O* atoms equals 1.7, 1.6 and 1.4 a.u. respectively. Outside the atomic spheres, we use the plane wave basis with cutoff of $R_{.M.T}{}^{*}Kmax$ equals 9.0. For the Brillouin zone integration, we use a mesh of 1000 k-points to ensure convergence and total energy minimization of the compound. The electronic configurations of the valence electrons of the constituents' ions are, [*Ni*]: $3p^6\ 3d^8\ 4s^2$, [*Fe*]: $3p^6\ 3d^6\ 4s^2$, [*O*]: $2s^2\ 2p^4$. The energy separation between valence and core states was set to —8 Ry. The charge convergence was set to $0.001e$.

3. Results and discussions

3.1. Structural properties

The general formula of spinel structure is AB_2O_4 where the O^{2-} anions are constructed from a face-centered cubic cell (CFC). These atoms are surrounded by the cations (A^{2+}) and (B^{3+}) respectively. For the normal spinel structure, the CFC sites of the tetrahedron (T_d) are occupied by 1/8 of the cations A^{2+} and on the other side 16/32 of the octahedral sites (*Oh*) are occupied by the cations B^{3+} (figures 1(a)–(c)). Another possible structure that is observed experimentally is the inverse spinel structure (figures 1(f)–(h)). In this structure, the octahedral sites are distributed between the cations B^{3+} and A^{2+}, while the other half of the cations B^{3+} occupy the tetrahedral sites. The primitive cell of the normal spinel is 8 times smaller than that of the inverse spinel. The two structures can be written in the form $[A]_X\ [B_2]_Y\ O_4$ and $[B]_X\ [AB]_Y\ O_4$, where *X* and *Y* denote the (T_d) and (O_h) sites, respectively for the normal and inverse spinel structure.

The cubic system of the inverse $NiFe_2O_4$ spinel (see figures 1(g), (h)) with a space group *n* 227 with iron atoms occupy *8a* tetrahedral (T_d) sites, and nickel and iron atoms that occupy (O_h) sites are distributed on positions 16d (Wyckoff notation) [22]. X-ray diffraction (XRD) measurements performed by Lee [14] and West [23] reported that

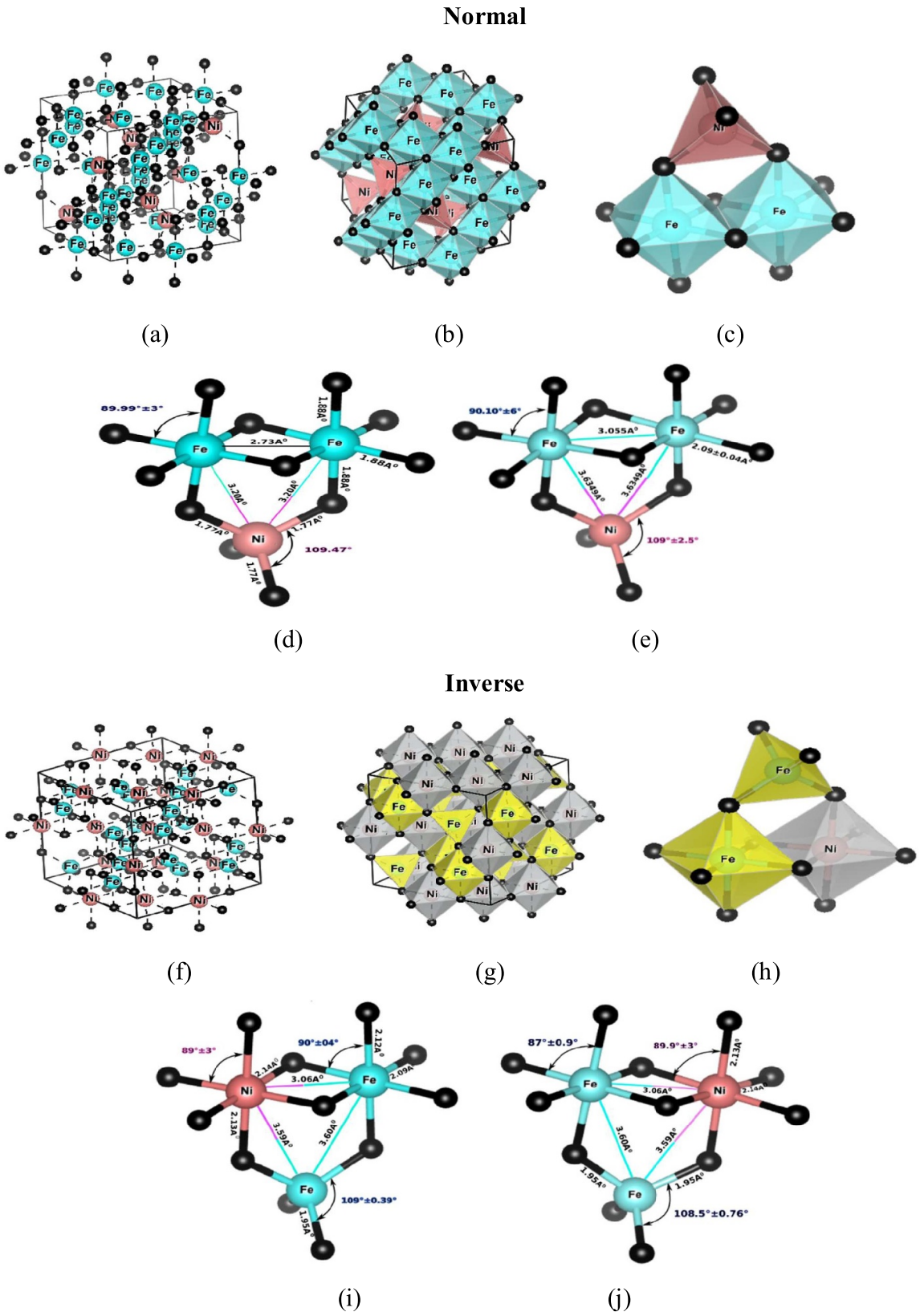

Figure 1. The crystal lattice structure of the $NiFe_2O_4$ compound; the octahedral and tetrahedral sites in normal (a)–(c) and inverse spinel (f)–(h) structures. The bond length and bond angles around the tetrahedral and octahedral sites of the normal spinel with the approximations (d) GGA and (e) GGA + U and inverse spinel of $NiFe_2O_4$ compound with the approximations (i) GGA and (j) GGA + U. *Ni*: pink, *Fe*: blue green, *O*: black.

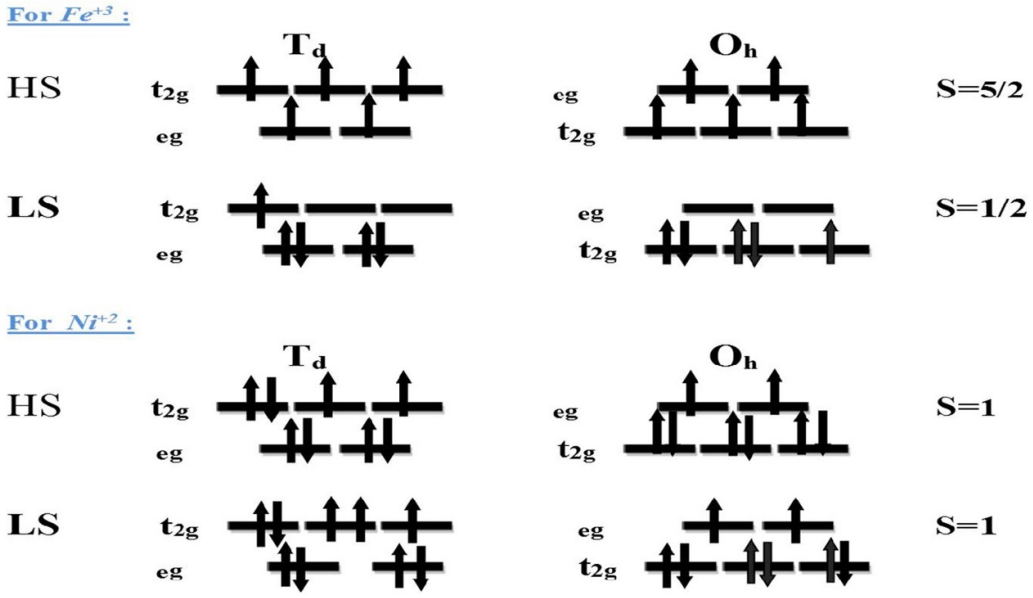

Figure 2. The *d* block of Fe^{3+} and Ni^{2+} cations in T_d and O_h environments with low-spin/high-spin (LS/HS) configurations of crystal field theory.

the lattice parameter of the cubic inverse spinel structure is 8.35 Å and the internal relaxation parameter u is 0.255. Examination of the elementary cell reveals a total of 56 atoms, 24 of which are the magnetic transition metals of iron and nickel. Consequently, several magnetic states are expected depending on the direction of rotation of the iron and nickel atoms (up or down) and the value of the magnetic moment of each atom. The magnetic moment measured is between 1.5 and 2.4 μ_B [24] and the compound is ferrimagnetic. Several factors can affect the magnetic moment of the compound. The most important factor is the atomic environment of the iron and nickel atoms. Moreover, oxygen atoms are surrounded by four metallic captions in a pseudo-tetrahedral structure. There are two species of oxygen that exist; namely, the oxygen d, denoted by O_{Fe}, is surrounded by three *Fe* atoms (two (O_h) sites and one (T_d) site) and one *Ni* atom, the second, denoted O_{Ni}, is surrounded by two *Fe* atoms (one on (O_h) site and one on (T_d) site) and two *Ni*. All oxygen atoms are bonded to three metal cations on (O_h) sites and one on a (T_d) site.

Several calculations have been carried out considering the GGA formalisms to determine the correctness of density functional theory (DFT) in describing the structure. The normal and inverse spinel structures with all possible initial spin arrangements have been studied [25]. The determination of the disposition of the spin of each metallic atom is achieved within the framework of the crystal field theory. The iron ions Fe^{3+} (formally d^5) in the octahedral and tetrahedral environments exhibit two configurations, the first is the high-spin HS and the second is low-spin LS as shown in figure 2. However, for the Ni^{2+} ions, this difference disappears. The nickel atoms have a partially filled d^8 level with two unpaired electrons for octahedral and tetrahedral symmetry at the level $\boldsymbol{e_g}$ or at the level $\boldsymbol{t_{2g}}$. As a result, crystals exhibiting this configuration have two magnetic sub-lattices [25]. To obtain a better understanding of this configuration, we analyzed the ferromagnetic arrangements of the octahedral cations of iron (O_h) and nickel *Ni* (O_h) and found that they form the first lattice with magnetic moments of 5 μ_B (d^5) and 2 μ_B (d^8), respectively. The iron atoms (T_d) that have a parallel magnetic moment of 5 μ_B (d^5), constituting the second lattice. Since the two sub-lattices are antiparallel, the total magnetic moment of the structure is 2 μ_B, in good agreement with experimental findings. Taking into account only the arrangement of the total atomic spin, the local magnetic moment indicates either spin up (↑) or down (↓) states. Three initial spin configurations can be considered for the normal spinel structure, namely a ferromagnetic arrangement (Ferro) in which all the magnetic moments of the atoms are parallel (↑ and ↑ for *Ni* (T_d) and *Fe* (O_h), respectively), a ferrimagnetic arrangement (Ferri) in which the magnetic moments of Fe^{3+} and Ni^{2+} are antiparallel (↓ and ↑ for *Ni* (T_d) and *Fe* (O_h), respectively) and an antiferromagnetic configuration (AntiF). For AntiF, three possible configurations (AntiF1, AntiF2 and AntiF3) are possible as presented in table 1. Furthermore, more initial total spin arrangements are taken into account because iron atoms have different octahedral and tetrahedral environments in the inverse phase. The above different spin configurations of the inverse spinel structure are summarized in table 1. Experimentally, the arrangements of the magnetic moment are ↑ ↓ ↑ for *Ni* (O_h), *Fe* (T_d) and *Fe* (O_h), respectively. The iron atoms are antiparallel in octahedral and tetrahedral sites results in a total magnetic moment of zero. The total magnetic moment of $NiFe_2O_4$ is therefore mainly due to nickel atoms *Ni* (O_h). Non-polarized spin calculations are also performed to assess the effects of spin on the structure.

3.1.1. Total energy calculations, magnetic phase stability. Previous attempts to use local density approximation (LSDA) [26] have failed to describe the magnetic properties of this structure adequately. For instance, a lattice parameter equal

Table 1. Spin arrangements of the normal spinel structure ($Ni(T_d)/Fe(O_h)$) and inverse structure ($Ni(O_h)/Fe(T_d)/Fe(O_h)$).

Magnetic States	Normal		Inverse		
Site	$Ni(T_d)$	$Fe(O_h)$	$Fe(T_d)$	$Ni(O_h)$	$Fe(O_h)$
Ferro	↑	↑	↑	↑	↑
Ferri	↓	↑	↓	↑	↑
AntiF1	Ni_1 Ni_2 ↑ ↓	Fe_1 Fe_2 Fe_3 Fe_4 ↑ ↓ ↑ ↓	Fe_1 Fe_2 ↑ ↓	Ni_1 Ni_2 ↑ ↓	Fe_3 Fe_4 ↑ ↓
AntiF2	Ni_1 Ni_2 ↑ ↓	Fe_1 Fe_2 Fe_3 Fe_4 ↓ ↑ ↑ ↓	Fe_1 Fe_2 ↑ ↓	Ni_1 Ni_2 ↓ ↑	Fe_3 Fe_4 ↑ ↓
AntiF3	Ni_1 Ni_2 ↑ ↓	Fe_1 Fe_2 Fe_3 Fe_4 ↑ ↑ ↓ ↓	Fe_1 Fe_2 ↑ ↑	Ni_1 Ni_2 ↓ ↑	Fe_3 Fe_4 ↓ ↓

Table 2. Calculated atomic positions (fractional coordinates) of the spinel $NiFe_2O_4$ compound using the GGA and GGA + U approximations.

The compound		*GGA*		*GGA + U*
$NiFe_2O_4$227_$Fd\bar{3}\,m$	Normal (Ferri)	***Ni (Tetra)***: 0.125,0.125, 0.125	Normal (Antif2)	***Ni***: 0.125,0.125, 0.125
		Fe (Octa): 0.5, 0.5, 0.5		***Fe***: 0.5, 0.5, 0.5
		O (Octa): 0.2570, 0.2570, 0.2570		***O***: 0.2570, 0.2570, 0.2570
		O(Octa): (0.25, 0.25, 0.25) [14] DFT		***O(Octa):*** (0.25, 0.25, 0.25) [14] DFT
		O(Octa): (0.25, 0.25, 0.25) [25, 29, 30] **Exp**		***O(Octa):*** (0.25, 0.25, 0.25) [25, 29, 30] **Exp**
	Inverse (Ferri)	***Fe (Tetra):*** 0.125, 0.122,0.125	Inverse (Ferri)	***Fe (Tetra):*** 0.125, 0.122,0.125
		Ni (Octa): 0.5, 0,0		***Ni (Octa):*** 0.5, 0,0
		Fe (Octa): 0.75,0.25, 0		***Fe (Octa):*** 0.75,0.25, 0
		O(Octa): 0.2554, 0.2523, 0.2554		***O(Octa):*** 0.2554, 0.2523, 0.2554
		O(Octa): (0.25, 0.25, 0.25) [14] DFT		***O(Octa):*** (0.25, 0.25, 0.25) [14] DFT
		O(Octa): (0.25, 0.25, 0.25) [25, 29, 30] **Exp**		***O(Octa):*** (0.25, 0.25, 0.25) [25, 29, 30] **Exp**

to 7.92 Å and total magnetic moment of 4 μB in the ferromagnetic case and that the normal spinel structure is more stable than the inverse one have been reported using the LSDA method. Consequently, we use the GGA approximation to describe the structural properties as well as the electronic and magnetic properties of inverse spinel structure instead of LSDA.

We performed self-consistent calculations within the framework of DFT for the properties of the inverse spinel $NiFe_2O_4$ compound. Although our results were in good agreement with some available experimental results, we seek to increase the accuracy of our calculations by implementing the DFT + U method, which includes the Hubbard parameter to account for the presence of '*d*' orbitals of both *Ni* and *Fe* atoms. The theoretical method proposed by Madsen [16] and Anisimov [17] allows the direct calculation of the Hubbard parameter U for both *Ni* and *Fe* atoms in both octahedral and tetrahedral sites. We found that U exhibits the following values: U (Fe_{Tetra}) = 6.569 eV, U (Fe_{Octa}) = 6.961 eV, U (Ni_{Octa}) = 5.469 eV, U (Ni_{Tetra}) = 5.107 eV. The LDA values for U of iron and nickel are 4.5 eV and 4 eV, respectively. Our results strongly disagree with the values obtained by San *et al* using the LDA approximation [27]. The study of Christopher J *et al* work reported U_{eff} of 4.5 eV for all *Fe* and 6.0 eV for all *Ni* atoms [28]. Another study performed by Anubhav Jain *et al* [29] reported U values equal to 4.0 eV and 6.0 eV for *Fe* and *Ni,* respectively.

The major part of this work is geared towards exploring the extraordinary features of crystal structure of the spinel compound $NiFe_2O_4$. In order to optimize the structural parameters, the total energy minimization approach is used to fully relax the face-centered cubic phase (CFC). The atomic positions are followed by minimizing the total energy of the unit cell and the Hellmann–Feynman forces on each atom. Table 2 lists the atomic positions of all atoms calculated using the GGA and GGA + U approximations for the most stable phases of the normal and inverse structure. The numbers within the brackets represent the DFT and the experimental references [14, 25, 29, 30]. The calculated data are in good agreement with previous experimental and theoretical findings [14, 25, 29, 30]. In order to obtain the ground state of the $NiFe_2O_4$ compound and to find the most favorable magnetic state, we compute the

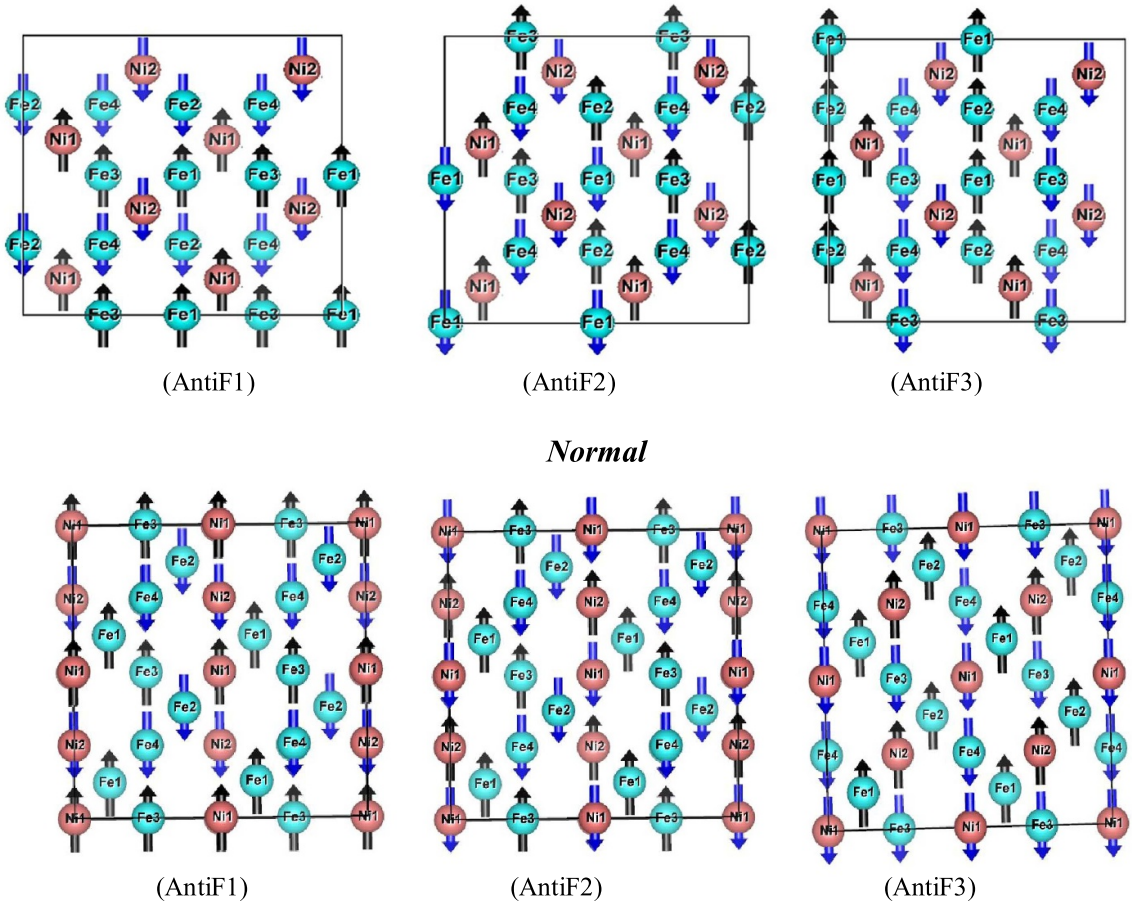

Figure 3. The possible antiferromagnetic configurations of *Fe* and *Ni* in a face-centered cubic phase $NiFe_2O_4$ cell.

total energy E of the unit cell at different volumes V and fit the data with the Murnaghan equation of state (EOS) [31] for six different magnetic configurations (one configuration for each ferromagnetic (Ferro), Ferrimagnetic (Ferri) and paramagnetic (PM) and three configurations for antiferromagnetic arrangement (AntiF1, AntiF2, AntiF3) using GGA and GGA + U approximations (see figure 3).

Using the GGA approximation, we found that normal and inverse spinels adopt the ferrimagnetic structure as the most stable magnetic structure as shown by figures 4(a) and (b). However, by using the GGA + U approximation, the normal spinel exhibits the second antiferromagnetic configuration (AntiF2) as the most stable magnetic structure as shown in figure 4(d), whereas the ferrimagnetic structure is found to be the most stable for the inverse spinel as shown in figure 4(e). In addition, figure 4(f) shows that the inverse ferrimagnetic phase is the most stable phase and that the total energy of nickel ferrite decreases as the degree of inversion increases.

Table 3 lists the calculated optimized quantities such as the lattice constant, the compressibility module and the minimum total energy and the volume, calculated using GGA and GGA + U methods. The values of the lattice parameters, magnetic parameters and the compressibility modulus of nickel ferrite equilibrium parameters obtained using GGA approximation agree well with the corresponding experimental values. To the best of our knowledge, the experimental value of bulk modulus has not been reported yet. However, previous experimental tests reported that spinel compounds have a global modulus of around 180 to 200 GPa [13]. Our calculations yield the bulk modulus $B = 189.18$ GPa) (see table 3) in excellent agreement with previously reported experimental values.

The Coulomb attraction between the oxygen ions and the iron ions Fe^{3+} at the octahedral site is stronger than that at the tetrahedral site, since the tetrahedral site has a smaller space than that of the octahedral site. Therefore, Ni^{2+} ions prefer the octahedral site from the point of view of the size effect. The radius of Fe^{3+} ions equals 0.64 Å [32], smaller than that of Ni^{2+} that has a radius of 0.69 Å. Total energy calculations show that the energy of the normal spinel is much larger than that of the ideal inverse spinel. The values obtained are 0.72 eV (2.34 eV) using GGA (GGA + U), respectively. Thus, the contribution from size effect is dominant over that of the Coulomb effect.

Table 3 lists the obtained optimized parameters as well as the available theoretical and experimental data. As presented by table 3, the GGA values of $a = 8.3534$ Å and $u = 0.2554$

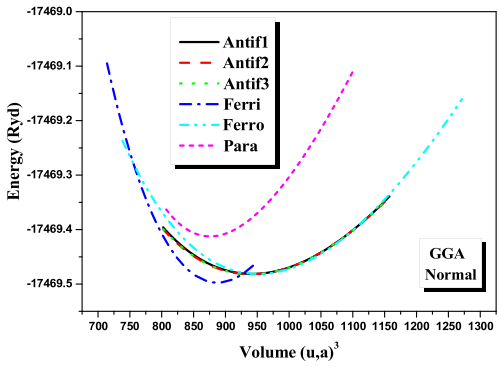

(a)

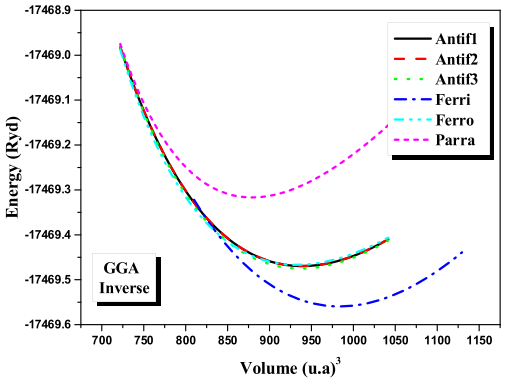

(b)

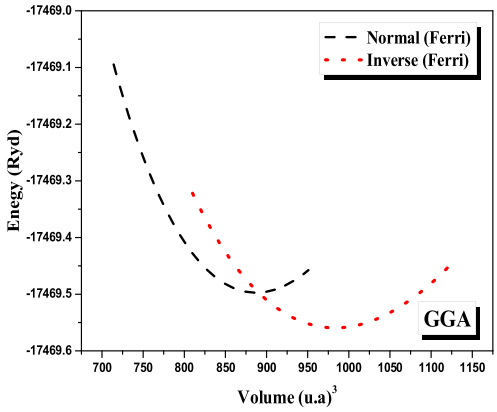

(c)

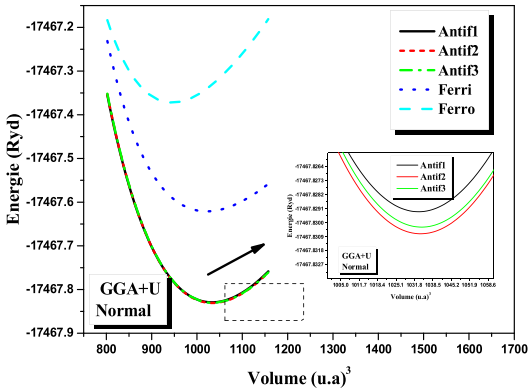

(d)

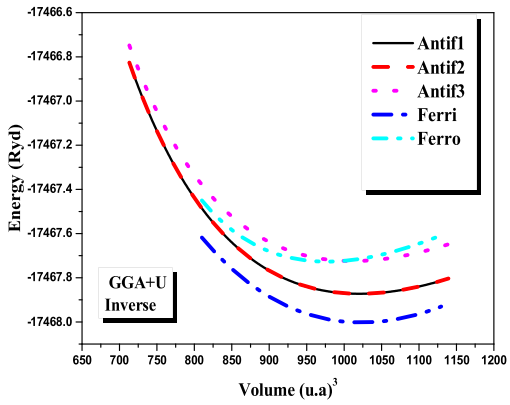

(e)

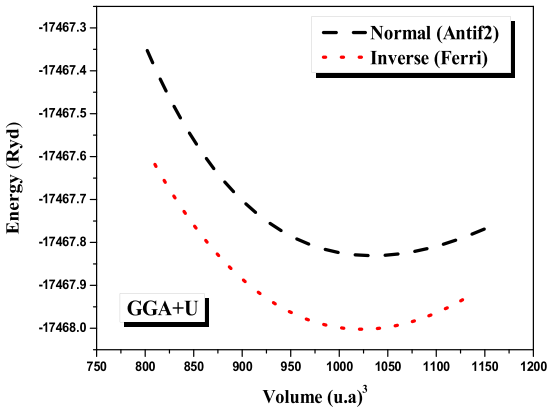

(f)

Figure 4. Comparison between the total energies as a function of the volume in antiferromagnetic, ferromagnetic, ferrimagnetic and paramagnetic states of the spinel $NiFe_2O_4$ compound in the normal and inverse cases with the GGA and GGA + U approximations.

of the inverse spinel phase are in excellent agreement with the experimental values ($a = 8.350$ Å and $u = 0.25$) [25, 29, 30]. For the normal spinel phase, the lattice parameter calculated using GGA + U is 1% higher than experimental value, whereas the value calculated using GGA approximation, 3% less than the experimental one.

The various details of the lengths and angles of bonds of the structures in the tetrahedral and octahedral sites are shown

Table 3. The lattice parameter values $a\,(A^{\circ})$, bulk modulus $B\,(GPa)$ and its derivative $B\prime$, the minimum energy $E_{min}\,(Ry)$ and the volume V_0.

The compound	Parameters	*GGA*		*GGA + U*	
		Normal	Inverse	Normal	Inverse
$NiFe_2O_4 227\_Fd\bar{3}\,m$	*a (our work)*	8.07	8.35	8.49	8.46
	a (exp)	8.35 Å [25, 29, 30]	8.35 Å [25, 29, 30]	8.35 Å [25, 29, 30]	8.35 Å [25, 29, 30]
	$\frac{\Delta a}{\mathbf{a}}\big\vert_{\mathrm{Exp}}$	−3.31	3.61	1.81	4.87
	$B\,(GPa)$	272.92	189.18 179–182 [14] DFT	170.49	208.15
	B'	2.68	2.13	4.46	1.96
	$V_0\,(Å)^3$	131.44	145.72	153.17	151.56
	$E_{min}\,(Ry)$	−17 469.49	−17 469.55	−17 467.83	−17 468.00

in figures 1(d), (e), (i) and (j). As figures 1(d), (e) show, no local distortion at the tetrahedral site of the normal structure is observed, as confirmed by the ideal spinel value of 109.47° (106.74°–111.90°) for the angle *O–Ni–O* calculated using GGA (GGA + U) approximations. Furthermore, our calculations indicate a slight local distortion on the octahedral site. The angle of the *O–Fe–O* bond is found between 86.64° and 93.35° (83.90° and 96.31°) using GGA (GGA + U), deviates from the ideal value of 90°. The results show that the *O–Ni–O* atoms tetrahedral coordination angles (109.47°) remain approximately constant [33].

The angle of the *Ni–O–Fe* bond is found to be 122.92° (126.42°) using GGA (GGA + U) slightly deviates from the ideal value of 125°. Moreover, the bond length of *Ni-O* is found to be 2.03 ± 0.03 Å, and the bond length of *Fe-O* is found to be 2.0132 ± 0.14 Å using GGA + U method. Using GGA approximation yields a bond length of *Ni-O* (1.77 Å) for the tetrahedron and *Fe-O* (1.88 Å) for the octahedron indicating a slight deviation from the ideal values for octahedral and tetrahedral bonds calculated using GGA + U approximation.

For the inverse spinel structure, our calculations indicate (See figures 1(i), (j)) a small tetragonality confirmed by the slight elongations of the *Ni–O* bonds along the *z* direction and *Fe–O* bonds contraction, along the same direction with respect to the same bonds in the (xy) planes.

Moreover, bond angles values shown in figures 1(i), (j) indicate a distortion associated with *Ni* atoms in the octahedral sites. The angle of the *O–Ni* (O_h)*–O* bond is found to be 89° ± 3° and the angle of the *O–Fe* (O_h)*–O* bond is found to 90.4° ± 2°, deviating slightly from the ideal spinel bond angle of 90 °. On the other hand, the angle of *Fe* (O_h)*–O–Fe* (T_d) bond is found to 124.06 ° and that of the $Ni\,(O_h) - O - Fe$ (T_d) bond is found to be 123°. Both deviate considerably from the ideal spinel value of 125°. Other bond lengths and angles are listed in table 4.

Table 5 summarizes the values of lattice parameters *a*, internal oxygen parameter *u*(*Oh*), energy variation, as well as the total and local magnetic moments of the normal and inverse spinel structures using the GGA and GGA + U methods. Table 5 also lists the experimental data (a = 8.35 a (Å), u(Oh) = 0.255, 1.5 < μtot < 2.4 μ_B) [25, 29, 30].

In addition, table 5 clearly demonstrates that when using GGA approximation, the normal spinel structure exhibits a ferromagnetic structure with atoms characterized by low magnetic spin moments of values ($\mu\,(Ni\,(T_d)) = -0.61\ \mu_B$ et $\mu\,(Fe\,(O_h)) = +1.22\ \mu_B$). The magnetic moment of oxygen is vanishingly small (approximately + 0.03 μ_B). For the normal ferrimagnetic spinel, a low-spin structure was also obtained with local magnetic moments of ≈ − 0.96 μ_B and ≈ + 1.19 μ_B for *Ni* (T_d) and *Fe* (O_h), respectively.

Careful examination of table 5 indicates that the inverse ferrimagnetic phase using GGA approximation exhibits lattice parameters that are very close to previous DFT values. For other spin configurations, the difference between the value of lattice parameter obtained from our work and previous DFT values is about 0.15 Å. We found that local magnetic moments on the atoms are respectively + 1.42/−3.31/+3.51/+0.03 μ_B for *nickel* (O_h), *iron* (T_d), *iron* (O_h) and *O*. The non-magnetic structure and the fact that energy of the normal spinel is −17 469.41 Ryd and that of the inverse spinel is −17 469.31 Ryd confirms that normal phase is more stable than the inverse. Finally, our results indicate that the lattice parameters of non-magnetic structure are smaller than those of the magnetic structure.

3.2. Electronic and magnetic properties

To obtain a deeper insight into the electronic and magnetic behaviors of a material, it is necessary to calculate the dispersion equation. In other words, the electronic band structure using points and directions of high symmetries in the first Brillouin zone are required. The energy bandgap can then be extracted from the electronic and structure by measuring the difference between the valence band maximum (VBM) and the conduction band minimum (CBM).

The band structure of the inverse spinel $NiFe_2O_4$ compound along the directions of highest symmetries in the first *Brillouin* zone is obtained using the GGA and mBJ, GGA + U and mBJ + U approximations. The *Fermi* E_F level is represented by a horizontal dotted line set to zero. The values of bandgap energies obtained from band structures are listed in table 6. As can be clearly seen from figures 5(a)–(b) using the GGA approximation, the $NiFe_2O_4$ compound exhibits a metallic character in both majority and minority spin configurations. Conversely, as can be seen from figures 5(c)–(d), by using the GGA + U approximation, the $NiFe_2O_4$ compound adopts a semiconductor character for the majority spin configurations with a bandgap along the direction Λ- $\Gamma\rightarrow$ W-L. For the minority spins, the VBM is located in the direction Λ- Γ and the CBM is located in the direction Λ- Γ, indicating that

Table 4. Selected interatomic distances (Å) and angles (deg) in the $NiFe_2O_4$ compound.

The compound $NiFe_2O_4$					
		GGA		*GGA + U*	
Interatomic distances and angles		Normal	Inverse	Normal	Inverse
Interatomic distances	*Ni-Fe*	3.20935 (×2)	3.06634 (×1)	3.63484 (×1)	3.59002 (×1)
			3.59002 (×1)	3.63495 (×1)	3.06634 (×1)
	Ni-O	1.77029 (×4)	2.13176 (×4)	2.03213 (×1)	2.13176 (×4)
			2.14882 (×2)	2.03235 (×1)	2.14882 (×2)
				2.05811 (×1)	
				2.06055 (×1)	
	Fe-Fe	2.73694 (×1)	3.60126 (×1)	3.05512 (×1)	3.60126 (×1)
	Fe-O	1.88246 (×6)	1.95209 (×2) Tetra	2.01446 (×1)	1.95209 (×2) Tetra
			1.95491 (×2) Tetra	2.13459 (×1)	1.95491 (×2) Tetra
			2.12157 (×4) Octa	2.13381 (×1)	2.12157 (×4) Octa
			2.09756 (×2) Octa	2.04072 (×1)	2.09756 (×2) Octa
				2.14188 (×1)	
				2.14001 (×1)	
The angles (deg)	*O-Fe-O*	86.64 (×4)	87.44 (×2) Octa	96.31 (×1)	87.44 (×2) Octa
		93.35 (×4)	92.55 (×2) Octa	96.30 (×1)	88.38 (×2) Octa
			91.61 (×2) Octa	83.90 (×1)	91.61 (×2) Octa
			88.38 (×2) Octa	84.57 (×1)	92.55 (×2) Octa
			109.54 (×2) Tetra	84.56(×1)	109.54 (×2) Tetra
			108.76 (×1) Tetra	84.09 (×1)	108.76 (×1) Tetra
				95.16 (×1)	
				95.15(×1)	
	O-Ni-O	109.47(×3)	86.79 (×2)	106.74 (×1)	93.20 (×4) 86.79 (×4)
			87.89 (×2)	111.88 (×1)	
			93.20 (×2)	111.90 (×1)	
			92.10 (×2)		
	Fe-O-Fe	93.2640 (×2)	124.0654 (×2)	91.3777 (×1)	124.0654 (×1)
				91.4184 (×1)	

the compound has an indirect bandgap. Employing the mBJ approximation, we can obviously seee that for the majority spin configurations, the compound has a semiconductor character with direct gap at Γ point, while for minority spins, the compound exhibits a semiconductor character with VBM located along the Δ-X direction and the CBM is located at the Γ point, indicating an indirect bandgap as can be seen from (see figures 5(e)–(f)). Furthermore, by implementing the mBJ + U approximation, the inverse spinel $NiFe_2O_4$ compound in the majority spins has a semiconductor character with the VBM located along the direction Λ- Γ and the CBM situated along the direction W-L, while for the minority spins the compound also has a semiconductor character, with VBM located at point Γ and CBM placed along the direction Λ- Γ as shown in figures 5(e)–(f).

Figure 6 shows the spin-polarized total density of states (TDOS) and partial spin density of states (PDOS) for face-centered cubic phase of the spinel compound $NiFe_2O_4$, using approximations GGA, GGA + U. Obviously, TDOS of up and down spins are not symmetrical. To determine the orbital nature (*s, p* or *d*) of the main peaks of TDOS, PDOS are analyzed to determine the contribution of each atomic orbit to a given energy band.

In spinel oxide systems, the determination of electronic and magnetic properties is based on the configuration of *d* electrons at different cation sites. This electronic configuration depends on the intra-atomic exchange field (EF) and the relative forces of the crystal field (CF) proposed by the theory of the crystal field [34]. For tetrahedral crystal field, levels $\mathbf{t_{2g}}$ are higher than $\mathbf{e_g}$ levels due to the direct repulsive electrostatic force between the d_{xy}, d_{yz} and d_z environmental anionic orbitals. However, if the environment order is inversed, orbitals d_{z^2} and $d_{x^2-y^2}$ are repelled directly. Thus, there are two possible electronic configurations, namely the high-spin (CF < EF) or low-spin (CF > EF) [33]. Levels $\boldsymbol{e_g}$ associated with octahedral sites, for instance, splits into two levels with the orbit $d_{x^2-y^2}$

at energy greater than d_{z^2} and the level $\mathbf{t_{2g}}$ splits into a higher-level d_{xy} and a doubly degenerate lower level (d_{zx}). The spacing of these energy levels depend on the forces of the crystal and the exchange fields.

In inverse spinel, the PDOSs shown in figures 6(a), (b) indicate that in the tetrahedral and octahedral sites, *Ni* is in the Ni^{2+}, and that iron is in Fe^{3+} state. The magnetic moment of iron Fe^{3+} is canceled since the spin in octahedral sites is always antiparallel to that of the tetrahedral sites. Thus, the net contribution to the magnetic moment comes from Ni^{2+} yielding a net magnetic moment of 2 μ_B per $NiFe_2O_4$ formula. The calculated magnetic moments (μ_B) of *Ni* and *Fe* atoms and the total magnetic moment of the compound are listed in table 5. The *GGA* calculation of the band structure of the

Table 5. The lattice parameter values $a\,(A^{\circ})$, internal oxygen parameter $u(Oh)$ and the energy variation, as well as the total and local magnetic moments.

	Magnetic States		a (Å)		$u(Oh)$		ΔE (eV)	μ_{Total}	μ_{local}
			Our work	DFT [14]	Our work	DFT [14]			
GGA	Normal	Ferri	8.07	8.14	0.2570	0.26	The stable structure	3.99 3.2 [14]	0.96/1.19 (Ni_T/Fe_O) − 0.69/ + 1.92 (Ni_T/Fe_O) [14]
		Ferro	8.26	8.12	0.2570	0.26	0.207 + 0.05 [14]	1.91 4.0 [14]	−0.61/1.22 (Ni_T/Fe_O) + 1.08/ + 1.31(Ni_T/Fe_O) [14]
		Parra	8.03	8.09	0.2570	0.26	1.15	/	/
		Antif 1	8.23		0.2561		0.213	0	0
		2	8.23		0.2693		0.203	0	0
		3	8.23		0.2570		0.204	0	0
	Inverse	Ferri	8.35	8.32	0.2554	0.25	The stable structure	2 2.0 [14]	−3.31/1.42/3.51($Fe_T/Ni_O/Fe_O$) + 1.33/ − 3.40/3 + .70 ($Fe_T/Ni_O/Fe_O$) [14]
		Ferro	8.20	8.22	0.2554	0.25	−0.109 + 0.04 [14]	−0.96 4.0 [14]	2.95/-1.32/3.25 ($Fe_T/Ni_O/Fe_O$) − 1.11/3 + .51/ + 1.37 ($Fe_T/Ni_O/Fe_O$) [14]
		Parra	8.04	8.08	0.2554	0.25	3.29	/	/
		Antif 1	8.22		0.2610		1.221	0	0
		2	8.22		0.2612		1.221	0	0
		3	8.21		0.2652		1.146	0	0
GGA + *U*	Normal	Ferri	8.45		0.2570		2.850	3.99	−1.90/3.24(Ni_T/Fe_O)
		Ferro	8.24		0.2570		6.241	4.00	1.64/1.014(Ni_T/Fe_O)
		Antif 1	8.49		0.2561		0.0014	0	0
		2	8.49		0.2693		The stable structure	0	0
		3	8.49		0.2570		0.0058	0	0
	Inverse	Ferri	8.46		0.2554		The stable structure	2	−3.88/1.69/3.98($Fe_T/Ni_O/Fe_O$)
		Ferro	8.33		0.2554		3.747	2	3.87/-1.67/0.87($Fe_T/Ni_O/Fe_O$)
		Antif 1	8.45		0.2610		1.768	0	0
		2	8.45		0.2612		1.770	0	0
		3	8.42		0.2652		3.784	0	0

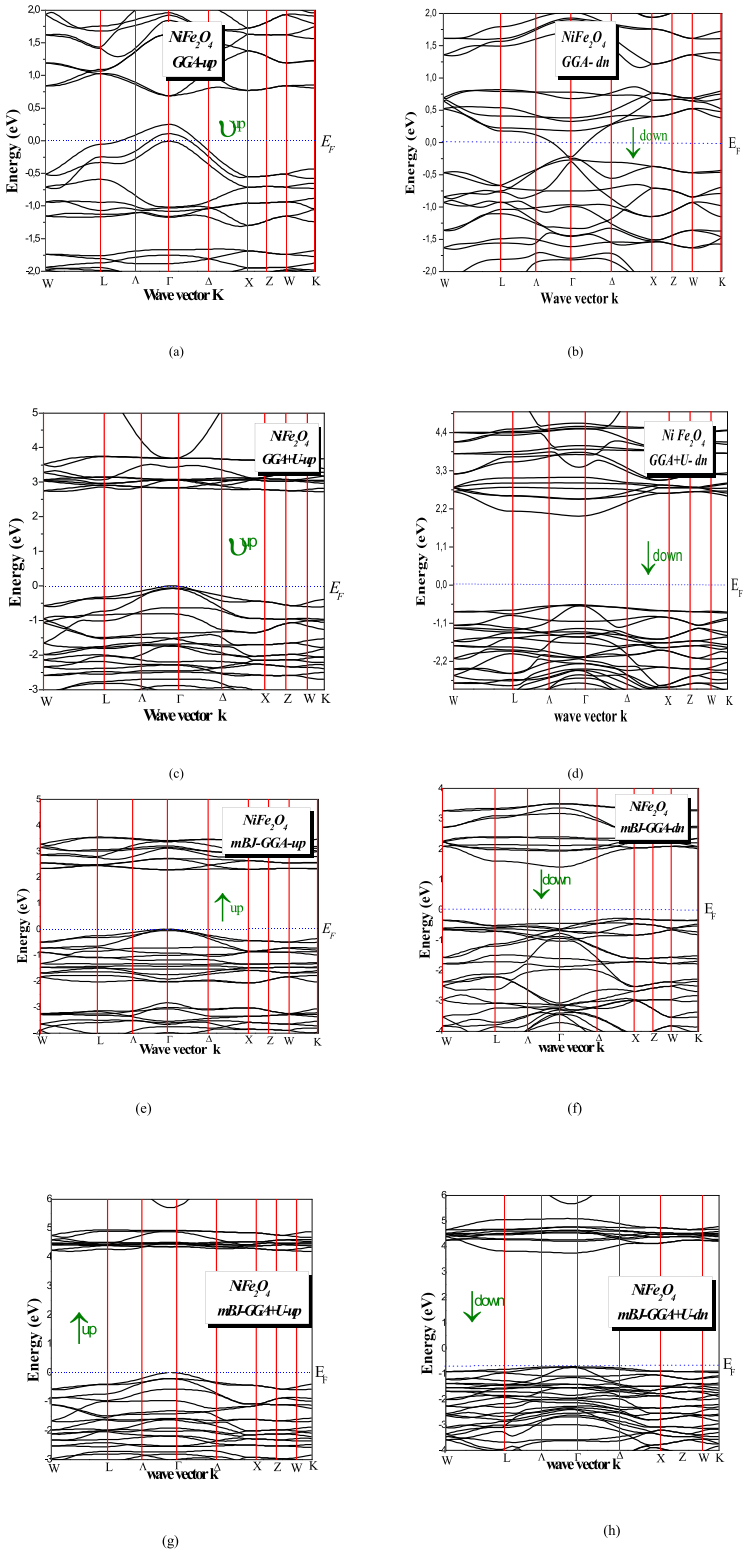

Figure 5. The band structure of inverse spinel $NiFe_2O_4$ compound calculated using the GGA, GGA + U, mBJ-GGA, and mBJ-GGA + U approximations.

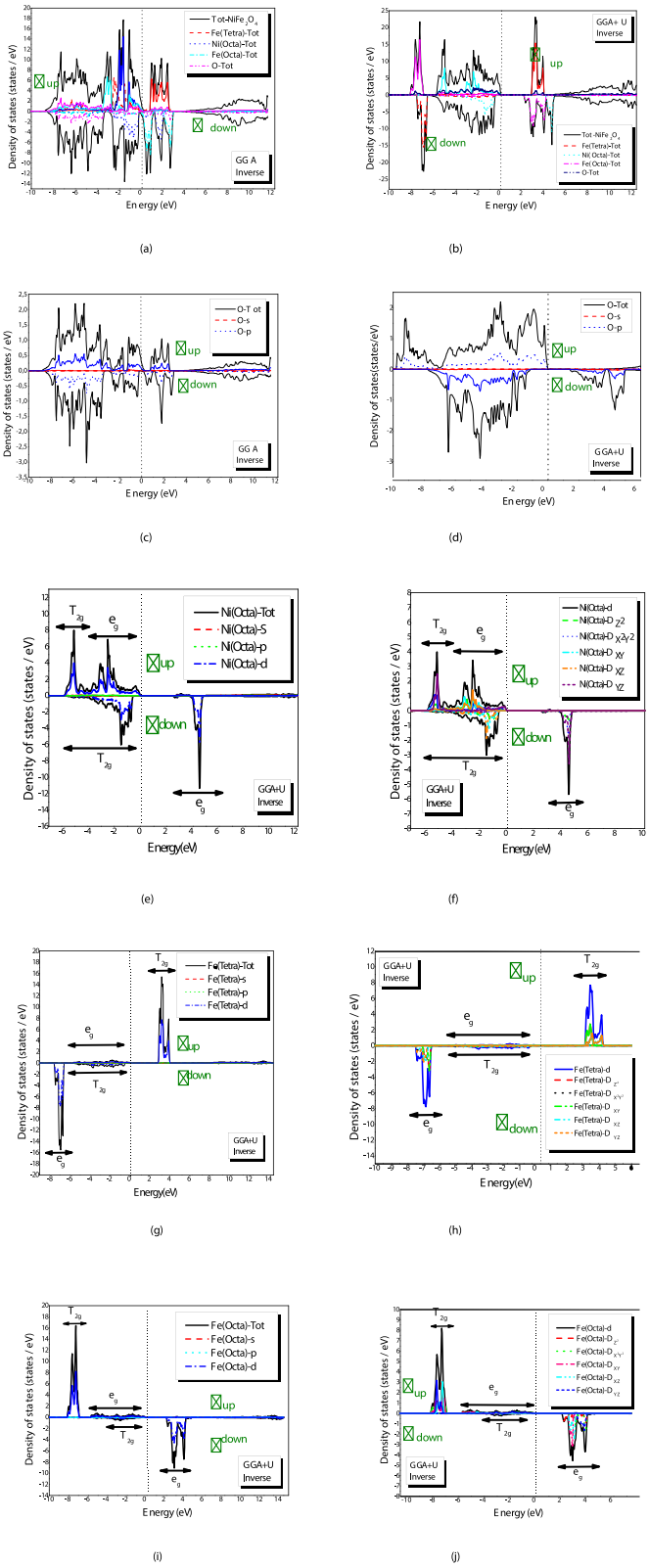

Figure 6. The total and partial densities of states of the inverse spinel $NiFe_2O_4$ compound in *CFC* structure using the GGA and GGA + U approximations.

Table 6. The values of energy gaps (eV), ε_1 (0) and n (0) for the $NiFe_2O_4$ compound in the CFC structure using GGA, GGA + U and mBJ and mBJ + U approximations.

Spinel	The Hubbard parameter (eV)	Spins	*Eg* (eV) *GGA*	*GGA + U*	*mBJ*	*mBJ + U*	$\varepsilon_1(0)$ *GGA + U*		$n(0)$ *GGA + U*	
$NiFe_2O_4 Fd\bar{3}m$	$U(Fe_{Tetra}) = 6.56901$	Up	0	2.718	2.289	4.172	Up	2.046	Up	1.43
	$U(Fe_{Octa}) = 6.96148$	Down	0	2.550	1.566	4.455	Down	3.48	Down	1.86
	$U(Ni_{Tetra}) = 5.10715$						Total	4.53	Total	2.12
	$U(Ni_{Octa}) = 5.46954$									

inverse spinel $NiFe_2O_4$ reveals that it is a metal. Employing *GGA* + *U* with $U = 5.10$ eV for *Ni* (Tetra) and $U = 6.96$ eV for *Fe* (Octa), inverse spinel $NiFe_2O_4$ is found to exhibit a semiconducting character with a bandgap of 2.718 eV for the majority spins and 2.550 eV for the minority spins. To the best of our knowledge, no experimental studies addressing band structures of $NiFe_2O_4$ have yet been reported. The conductivity measurements [35] have been done in the interval of 0.45 eV for the $NiFe_2O_4$ compound. Based on the available experimental data, they concluded that the GGA + U approximation is sufficiently precise to determine the effects of the degree of inversion and stoichiometry and the distribution of cations on the magnetostrictive properties of spinel ferrites [36].

To obtain a deeper insight into the electronic structure of the inverse spinel $NiFe_2O_4$, we analyze the PDOS of each atomic orbital, and to show the role of the effect of strong correlation on the insulating behavior, we plotted the partial densities of states using GGA and GGA + U.

The oxygen atoms in figures 6(c), (d) show that the up and down spin states are almost symmetrical, leading to a weak local magnetic moment of + 0.03 μB (see table 5). Since *O-p* states occupy the E_F, it confirms the charge-transfer mechanism [37]. It is anticipated that for inverse spinel $NiFe_2O_4$ compound, the *d* orbitals will contribute the major part of the TPDOS around E_F. Thus, it is important to analyze the PDOS of the three constituent atoms, namely, *nickel* (O_h), *iron* (T_d) and iron (O_h).

The major contribution to TPDOS in the vicinity of the *Fermi* level comes from *d* orbital band of metallic atoms. It has been found that there is a correlation between the *d* block structures and the crystal field theory of *Ni* (O_h), *Fe* (T_d) et *Fe* (O_h) as demonstrated from their PDOS shown in figures 6(e)–(h). Figures 6(e), (f) show the PDOS of *Ni* (O_h). They indicate that all DOS (up) are located before the *Fermi* level and completely and for the DOS (down), the band $\boldsymbol{T_{2g}}$ is filled, yielding a local magnetic moment of + 1.7 μ_B (see table 5) consistent with the expected d^8 configuration of the crystal field theory. So, they are not affected by the on-site repulsion *U* [37]. Figures 6(g), (h) show PDOS of *Fe* (T_d). We found that all *DOS* (down) and $\boldsymbol{e_g}$ (up) are filled. The magnetic moment obtained equals −3.87 μ_B (see table 5), consistent with the expected d^5 spin configuration of crystal field theory. The *Fe* (T_d) states are away from the E_F both in GGA and GGA + U and hence have a negligible role in determining the insulating mechanism in this system [37]. Furthermore, figures 6(i), (j) show the PDOSs of *Fe* (O_h). We found that all the *DOS* (up) and the lower band of $\boldsymbol{T_{2g}}$ (down) are filled. The obtained total magnetic moment is found to be +3.99 μ_B (see table 5), indicating that these atoms exhibit high-spin configuration.

In summary, $NiFe_2O_4$ is a ferrimagnetic oxide at room temperature and has a high Curie temperature (850 K); the critical temperature of $NiFe_2O_4$ compound is 844 K [38], which is in good agreement with the experimental value. The magnetic order in this ferrite comes from several exchange interactions between different cations. There are mainly two couplings of super-exchange and one of double exchange. Super-exchange interactions take place via anions O^{2-}, by overlap between the *3d* orbitals of the two cations and the *2p* orbitals of intermediate oxygen. For an angle α greater than 90°, the super-exchange interaction gives an antiferromagnetic coupling. The strongest interaction is between sites *A* and *B,* which forms *A-O-B* angle of 125°. This interaction gives a strong antiferromagnetic coupling and, furthermore, a weaker antiferromagnetic coupling between the sites *A* and a weak ferromagnetic coupling between the sites *B* interacting by super-exchange. This super-exchange interaction is difficult to separate from the weak interaction by double exchange between the *B* sites. This last interaction is based on the direct transfer of an electron between the two cations at site *B*. For the ferrites $NiFe_2O_4$, the net magnetic moment (μ) comes from the sum of the contributions of all the magnetic interactions between different cations. The values of the magnetic moment calculated by the GGA + U, mBJ, and mBJ + U approximations are summarized in table 8. As table 7 indicates, the total magnetic moment of inverse spinel $NiFe_2O_4$ compound is 2 μ_B. The value obtained using the GGA approximation is found to be 1.91 μ_B. Table 7 indicates that the contribution of the *Fe* atom is much greater than that of the *Ni* atom at the *Fermi* level.

3.3. Optical properties

The optical parameters of inverse spinel $NiFe_2O_4$ compound can be determined from the complex dielectric function, $\varepsilon(\omega) = \varepsilon_1(\omega) + i\varepsilon_2(\omega)$, where $\varepsilon_1(\omega)$ and $\varepsilon_2(\omega)$are the real and the imaginary part of the dielectric function. The two parameters are calculated using [41]

$$\varepsilon_2(\omega) = \frac{8}{3\pi\omega^2}\sum_{nn'}\int_{BZ}|P_{nn'}(\mathbf{k})|^2\frac{dS_k}{|\nabla_k\omega_{nn'}(k)|}. \quad (1)$$

The above expression is expressed in Rydberg atomic units with $e^2 = 1/m = 2$ and $\hbar = 1$.

Table 7. Theoretical values of magnetic moments (m_0) calculated for the spinel $NiFe_2O_4$ compound using GGA, GGA + U, mBJ and mBJ + U approximations.

Spinel	*The moment* m_0 (μ_B/*f. u*)	*GGA*	*GGA + U*	*mBJ*	*mBJ + U*
$NiFe_2O_4$227_$Fd\bar{3}m$	Interstitial	−0.013	0.024	−0.207	−0.099
	Fe (*Tetra*)	−2.981 –3.46 [39]	−3.877 –3.97 [39] −3.98 [40]	−3.707	−4.152
	Ni (*Octa*)	1.322 1.36 [39]	1.683 1.58 [39] 1.55 [40]	1.690	1.832
	Fe (*Octa*)	3.278 3.71 [39]	3.990 4.11 [39] 4.01 [40]	3.864	4.215
	O	0.15	0.095	0.129	0.077
	Total	1.914 2.0 [14] DFT $1.5 < \mu_{tot} < 2.4$ [30–32] Exp	2.00	2.00	2.00

$\omega_{nn'}(k)$ is the photon energy (Ry). The element of the dipolar matrix $P_{nn'}(k)$ is defined from the initial $|nk\rangle$ and final $|n'k\rangle$ states with eigenvalues $E_n(k)$ and $E_{n'}(k)$. The difference of energy is given by $\omega_{nn'}(k) = E_n(k) - E_{n'}(k)$ and S_k is a constant energy surface, $S_k = \{k;\ \omega_{nn'}(k) = \omega\}$.

In the case of polarizability, $\alpha = \alpha_1 + i\alpha_2$, the above conditions are satisfied. Kramers–Kronig relations yield [42]

$$\alpha_1(\omega) = \frac{2}{\pi} P \int_0^{+\infty} \frac{\omega' \alpha_2(\omega')}{\omega'^2 - \omega^2} d\omega', \tag{2}$$

$$\alpha_2(\omega) = -\frac{2\omega}{\pi} P \int_0^{+\infty} \frac{\omega' \alpha_1(\omega')}{\omega'^2 - \omega^2} d\omega'. \tag{3}$$

Where ω is the frequency and P is the main part of the Cauchy integral, defined by

$$P = \lim_{\alpha \to 0} \int_{-\infty}^{\omega - a} \frac{\alpha(\omega')}{\omega' - \omega} d\omega' + \int_{\omega + a}^{+\infty} \frac{\alpha(\omega')}{\omega' - \omega} d\omega'. \tag{4}$$

The real part $\varepsilon_1(\omega)$ can be estimated from $\varepsilon_2(\omega)$ using the Kramers–Kronig expressions and given by [42]

$$\varepsilon_1(\omega) = \mathrm{Re}\,\varepsilon(\omega) = 1 + \frac{2}{\pi} P \int_0^{+\infty} \frac{\omega' \varepsilon_2(\omega')}{\omega'^2 - \omega^2} d\omega'. \tag{5}$$

The reflectivity$R(\omega)$, the absorption coefficient$I(\omega)$, refractive index $n(\omega)$, and extinction coefficient $k(\omega)$ in the crystal are related to the reflectivity at normal incidence by

$$R(\omega) = \frac{n + ik - 1}{n + ik + 1}, \tag{6}$$

$$I(\omega) = \sqrt{2}\omega \left[\sqrt{\varepsilon_1(\omega)^2 + \varepsilon_2(\omega)^2} - \varepsilon_1(\omega) \right]^{1/2}, \tag{7}$$

$$k(\omega) = I(\omega)/2\omega, \tag{8}$$

$$n(\omega) = \left(1/\sqrt{2}\right) \left[\sqrt{\varepsilon_1(\omega)^2 + \varepsilon_2(\omega)^2} + \varepsilon_1(\omega) \right]^{1/2}. \tag{9}$$

Figure 7(a) reports the evolution of the imaginary part of the complex dielectric function $\varepsilon_2(\omega)$, in the energy range [0–40] eV for the inverse spinel $NiFe_2O_4$ compound. The analysis of the densities of states and structures of energy bands allows us to identify the origins of the peaks of the imaginary part of the dielectric function. Furthermore, using the band structure, density of states and absorption spectra of the compound, different inter-band transitions can be interpreted. As the electric dipole transition retains the spin (the transitions are between electrons of the same spin), we have traced the optical responses corresponding to the spin electrons ↑ (majority) and spins ↓ (minority).

Analysis of this spectrum shows the existence of absorption peaks. We have identified two absorption peaks, indicated by b1 and b2, located at the energies 6.29 and 16.09 eV. These peaks (b1 and b2) are found in the ultraviolet region; the origin of these peaks can be attributed to the electronic transitions of the minority state of b1 and the electronic transitions of the majority state of b2. The absorption threshold (first critical point) of the dielectric function in the minority state of this compound occurs at energy 2.38 eV. This point represents the indirect optical transitions between VBM and CBM. The absorption threshold of the dielectric function in the majority state occurs at energy 4.55 eV. This point represents the optical indirect transitions between the VBM and CBM. Experimentally, $NiFe_2O_4$ shows indirect/direct optical band gaps around 1.52 eV/2.74 and 2.3 eV, for the ideal inverse spinel configuration [43].

The evolution of the extinction coefficient as a function of energy for the inverse spinel compound $NiFe_2O_4$ using GGA + U is shown in figure 7(b). The maximum value of the extinction coefficient observed corresponds to the energy 7.25 eV, which belongs to the ultraviolet region, and comes mainly from the interband transitions of minority states. This value corresponds to the zero of $\varepsilon_1(\omega)$

The real part of the dielectric function is obtained from the imaginary part $\varepsilon_2(\omega)$ by means of Kramers–Kronig transformations [44]. The variation of the real part of the dielectric function as a function of the energy of the inverse spinel compound $NiFe_2O_4$ using GGA + U is shown in figure 7(c). It shows that the real part increases as the photon

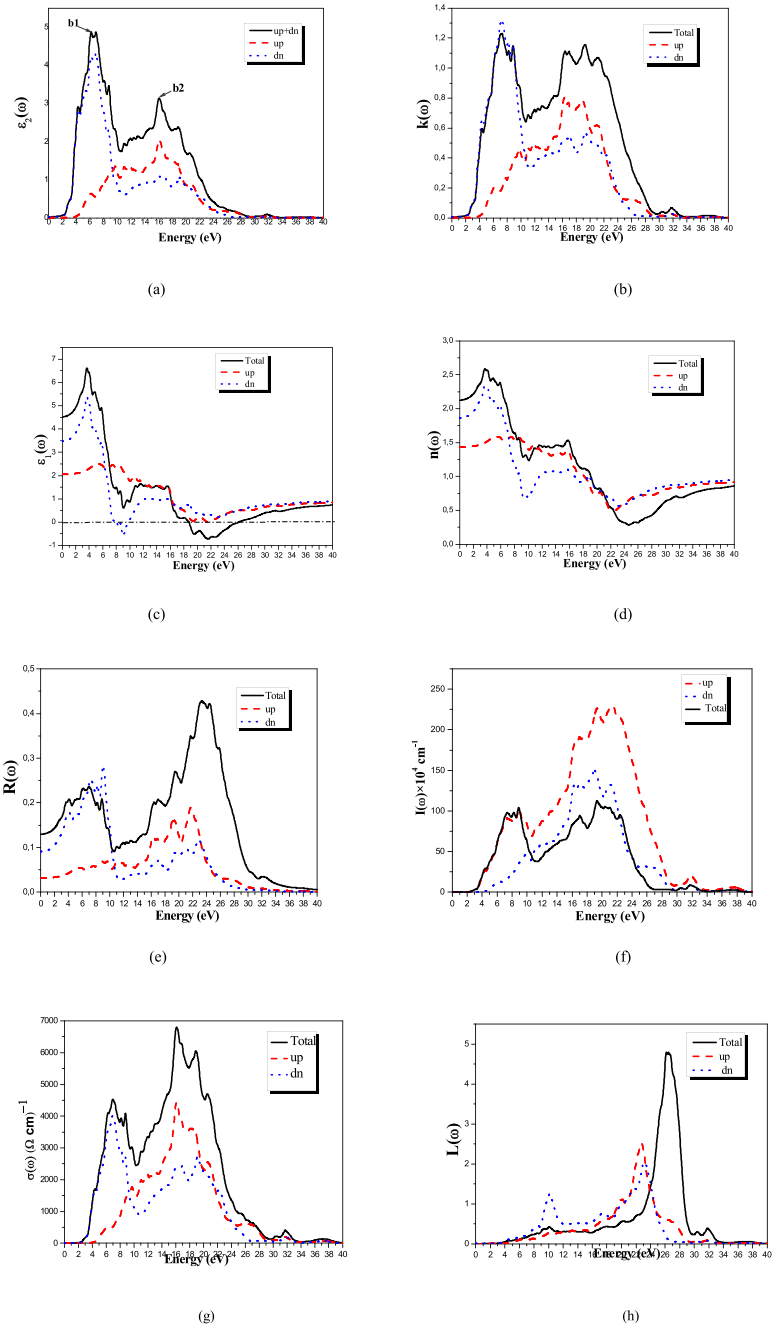

Figure 7. (a) Variation of the imaginary part of the dielectric function, (b) the extinction coefficient, (c) variation of the real part of the dielectric function, (d) the refractive index, (e) reflectivity spectra, (f) the absorption coefficient, (g) variation of the optical conductivity and (h) the energy loss function as a function of energy for the inverse spinel $NiFe_2O_4$ compound using the GGA + U approximation.

energy is increased, reaches the major peak and becomes zero at 18.73 eV. After crossing a minimum, it increases again reaching a second peak, and it becomes zero again at energy 26.10 eV. The origin of the intense peak in the calculated optical spectrum is formed by electronic excitations in the minority bands. The zero crossing of the spectra signifies the inexistence of the scattering. We note that the function vanishes for energy values at which dispersion is zero.

The static dielectric constant $\varepsilon_1(0)$ is obtained as the limit of the real part of the dielectric function approaches zero energy. We note that the small energy gap gives a large value of $\varepsilon_1(0)$. This can be explained by the Penn model [45]

$$\varepsilon_1(0) \approx 1 + \left(\frac{\hbar\omega_P}{E_g}\right)^2. \tag{10}$$

It is clear that $\varepsilon_1(0)$ is inversely proportional to E_g. We can determine the gap from this expression using the values of $\varepsilon_1(0)$ and plasma frequency ω_p. As far as optical applications are concerned, the refractive index is a very important optical property. This value determines the amount of light that will be reflected upon reaching the interface, as well as the critical angle of the total internal reflection in optical devices such as photonic crystals, waveguides and solar cells.

The refractive index that describes the behavior of an electromagnetic wave in a medium has been calculated. The spectra are shown in figure 7(d). It shows that the refractive index generally follows the shape of the real part. The zero frequency, static dielectric constants $\varepsilon_1(0)$ and $n(0)$ are calculated and listed in table 6.

Figure 7(e) shows the evolution of the refractive index as a function of energy for the inverse spinel compound $NiFe_2O_4$ using the GGA + U method. The curve of variation of the refractive index in the energy range [0–6] eV has a maximum at an energy of 3.95 eV. This maximum comes from the minority state. We also note that the value of the refractive index decreases as the frequency increases in the energy range (10–18 eV) and exhibits non-linear behavior.

By using the imaginary and real parts obtained from the frequency-dependent dielectric function, we can estimate other optical properties such as the absorption coefficient $I(\omega)$ and the reflectivity spectra $R(\omega)$.

For the minority states, this spinel has a small reflectivity starting at 9.09%. For the majority states, a small reflectivity starts at 3.13%, and the total reflectivity of this spinel is found to be 12.97% as can clearly be seen from figure 7(e). Figure 7(e) shows that total reflectivity increases at low energy and then decreases thereafter. This increase corresponds to the minority states. It increases again to reach the main peak at an energy of 23.30 eV. This maximum reflectivity results from the interband transitions corresponding to the majority states. Beyond this peak, the reflectivity spectrum decreases at high energies.

Figure 7(f) shows the total absorption coefficient of the inverse spinel compound $NiFe_2O_4$ for both majority and minority states as a function of photon energy using GGA + U method. We note that at low energies, the absorption coefficient increases considerably to reach its maximum value at higher energies. The strong peak is observed at 21.45 eV. The absorption coefficient $I(\omega)$ is large (10^4 cm^{-1}) and increases rapidly. The absorption spectra exhibit peaks in the energy range 162–163 eV.

The optical conductivity $\sigma(\omega)$ relates the oscillating electric field $E(\omega)$ with current density $j(\omega)$ [46]

$$j(\omega) = E(\omega)\sigma(\omega), \tag{11}$$

and as $\omega \to 0$, it converts to electrical conductivity. It has a direct relation to the imaginary part of the dielectric function. Its real part can be expressed as [47]

$$\sigma(\omega) = \frac{\omega}{4\pi}\varepsilon_2. \tag{12}$$

Several peaks corresponding to interband transitions are present in the optical conductivity spectrum as shown in figure 7(g). Sharp edges occur in the energy range 15–17 eV in the *ultraviolet* region.

Finally, energy loss function $L(\omega)$ can be deduced from the dielectric function. It can be described by

$$L(\omega) = \mathrm{Im}\left(-\frac{1}{\varepsilon(\omega)}\right). \tag{13}$$

This can also be rearranged as

$$L(\omega) = \left(\frac{\varepsilon_2(\omega)}{\varepsilon_1(\omega)^2 + \varepsilon_2(\omega)^2}\right). \tag{14}$$

Figure 7(h) shows $L(\omega)$ of the inverse spinel $NiFe_2O_4$ compound. The energy interval 24.462–28.53 eV is characterized by a significant energy loss. The highest peak of $L(\omega)$ is 26.40 eV. The main peak occurs when $\varepsilon_2(\omega)$ is very small and $\varepsilon_1(\omega)$ approaches zero again. The plasma frequency ω_p is the average peak of the energy loss function. Therefore, the plasma energy $\hbar\omega_p$ is calculated to be 26.40 eV.

4. Conclusion

In conclusion, self-consistent *ab initio* calculations are carried out within the framework of density functional theory (DFT) using the method of augmented plane waves plus the local orbital with the total potential (FP-APW + lo). The total energy minimization approach is implemented to investigate the phase stability of the inverse spinel $NiFe_2O_4$ compound. The total energy as a function of the volume for paramagnetic, ferromagnetic, ferrimagnetic and aAntiferromagnetic possible phases are plotted using the GGA and GGA + U approximations. Using the GGA approximation, the most stable state for the normal and inverse spinel compound is found to be the ferrimagnetic state, whereas the most stable state using the GGA + U approximation is found to be antiferromagnetic (configuration 2) for the normal and ferrimagnetic spinel of the inverse spinel. Our results are found to be in good agreement with previous studies. Implementing the GGA approximation, the calculated structural lattice parameters, magnetic parameters and the bulk modulus of nickel ferrite are found to be in good agreement with experimental values. The typical values of elastic modulus of spinel compounds lie in the range 180 to 200 GPa. We found the bulk modulus of inverse spinel to be B 189.18 GPa, in good agreement with previously reported results. Our calculations indicate that GGA is a good approximation for the study of bonding properties for this type of spinel. The bulk modulus of the inverse spinel $NiFe_2O_4$ compound is found to be 189.18 (208.15) GPa and the equilibrium volume of the unit cell V_0 = 145.72 (151.56) Å^3 using GGA and (GGA + U) approximations, respectively.

GGA, GGA + U, mBJ and mBJ + U approximations are employed to calculate the electronic properties of the inverse spinel $NiFe_2O_4$ compound. Using the GGA approximation, the compound is found to exhibit metallic character for both majority and minority spins. Using the GGA + U, mBJ and mBJ + U approximations, the compound demonstrates a semiconductor character for majority and minority spin configurations.

Ferrite nickel favors the inverse spinel phase with iron and nickel cations in either octahedral or tetrahedral sites taking the high-spin configuration. Furthermore, the values of atomic magnetic moment increase as the value of inversion parameter is decreased and the total magnetic moment of $NiFe_2O_4$ decreases. The total energy of the normal spinel is found to be

greater than that of the inverse spinel, indicating that the compound is more stable in the inverse spinel structure. The total magnetic moment of the compound is found to be 2 μ_B using the GGA + U method. The GGA approximation yields a magnetic moment of 1.91 μ_B. Our calculations indicate that contribution of the *Fe* atom to the magnetic moment is much greater than that of the *Ni* atom at the *Fermi* level. To characterize the inverse spinel $NiFe_2O_4$ compound optically, we calculate the real and imaginary part of the dielectric function, the absorption coefficients, reflectivity, the refractive index, the optical conductivity and the energy loss. The optical parameters are calculated, analyzed and interpreted to explore the potential of the spinel compound for optical and optoelectronic device applications. We believe that our comprehensive detailed analysis of structural, electronic, magnetic and optical properties of the novel inverse spinel $NiFe_2O_4$ compound should pave the way to explore this compound for a wide range of device applications.

Acknowledgments

This work is supported by the Algerian University research project (PRFU) under No. B00L02UN280120180002 and the General Directorate for Scientific Research and Technological Development (DGRSDT), Algeria.

ORCID iDs

Z Charifi https://orcid.org/0000-0003-3875-4716
H Baaziz https://orcid.org/0000-0003-4860-2740
A M Alsaad https://orcid.org/0000-0003-1721-1878

References

[1] Kodama T, Kato H, Chang S G, Hasegawa N, Tsuji M and Tamaura Y 1994 *J. Mater. Res.* **9** 462
[2] Marco J F, Gancedo J R, Gracia M, Gautier J L, Ríos E I, Palmer H M, Greaves C and Berry F J 2001 *J. Mater. Chem.* **11** 3087
[3] Anderson R M, Vestal C R, Samia A C and Zhang Z J 2004 *Appl. Phys. Lett.* **84** 3115
[4] Van Der Zaag P J, Ruigrok J J M and Gillies M F 1998 *Philips J. Res.* **51** 173
[5] Kim H J, Song I C, Sim J H, Kim H, Kim D, Ihm Y E and Choo W K 2004 *J. Appl. Phys.* **95** 7387
[6] Bakuzis A F, Skeff Neto K, Gravina P P, Figueiredo L C, Morais P C, Silva L P, Azevedo R B and Silva O 2004 *Appl. Phys. Lett.* **84** 2355
[7] Chen X M, Tang Y H, Chen I-W, Xu Z C and Wu S Y 2004 *J. Appl. Phys.* **96** 6520
[8] Dai Y R, Bao P, Zhu J S, Wan J G, Shen H M and Liu J M 2004 *J. Appl. Phys.* **96** 5687
[9] Bichurin M I, Filippov D A, Petrov V M, Laletsin V M, Paddubnaya N and Srinivasan G 2003 *Phys. Rev.* B **68** 132408
[10] Zheng H, Wang J, Lofland S E, Ma Z, Mohaddes-Ardabili L, Zhao T, Salamanca-Riba L, Shinde S R, Ogale S B and Bai F 2004 *Science* **303** 661
[11] Tanihara M, Suzuki Y, Yamamoto E, Noguchi A and Mizushima Y 2001 *J. Biomed. Mater. Res.* **56** 216
[12] Jiang W, Yang H-C, Yang S-Y, Horng H-E, Hung J C, Chen Y C and Hong C-Y 2004 *J. Magn. Magn. Mater.* **283** 210
[13] Hu G, Choi J H, Eom C B, Harris V G and Suzuki Y 2000 *Phys. Rev.* B **62** R779
[14] Kang J-S, Kim G, Lee H J, Kim D H, Kim H S, Shim J H, Lee S, Lee H, Kim J-Y and Kim B H 2008 *Phys. Rev.* B **77** 035121
[15] Nicolau P, Bunget I, Rosenberg M and Belciu I 1970 *IBM J. Res. Dev.* **14** 248
[16] Madsen G K H and Novák P 2005 *EPL Europhys. Lett.* **69** 777
[17] Anisimov V I and Gunnarsson O 1991 *Phys. Rev.* B **43** 7570
[18] Blaha P, Schwarz K, Madsen G K, Kvasnicka D and Luitz J 2001 Augment. Plane Wave Local Orbitals Program Calc. Cryst. Prop..
[19] Perdew J P, Burke K and Ernzerhof M 1996 *Phys. Rev. Lett.* **77** 3865
[20] Becke A D and Johnson E R 2006 *J. Chem. Phys.* **124** 221101
[21] Dudarev S L, Botton G A, Savrasov S Y, Humphreys C J and Sutton A P 1998 *Phys. Rev.* B **57** 1505
[22] Sands D E 1967 *Microchem. J.* **12** 134
[23] West A R 1999 *Basic Solid State Chemistry* (New York: Wiley)
[24] Bhosale A G and Chougule B K 2006 *Mater. Chem. Phys.* **97** 273
[25] Lüders U, Bibes M, Bobo J-F, Cantoni M, Bertacco R and Fontcuberta J 2005 *Phys. Rev.* B **71** 134419
[26] Perron H, Mellier T, Domain C, Roques J, Simoni E, Drot R and Catalette H 2007 *J. Phys. Condens. Matter* **19** 346219
[27] Sun Q-C, Sims H, Mazumdar D, Ma J X, Holinsworth B S, O'Neal K R, Kim G, Butler W H, Gupta A and Musfeldt J L 2012 *Phys. Rev.* B **86** 205106
[28] O'Brien C J, Rák Z and Brenner D W 2013 *J. Phys. Condens. Matter* **25** 445008
[29] Blöchl P E, Jepsen O and Andersen O K 1994 *Phys. Rev.* B **49** 16223
[30] Wyckoff R W G 1964 *Crystal Structures* (New York: Wiley)
[31] Murnaghan F D 1944 *Proc. Natl. Acad. Sci. U. S. A.* **30** 244
[32] Shannon R D 1976 *Acta Crystallogr.* A **32** 751
[33] Jong U-G, Yu C-J, Park Y-S and Ri C-S 2016 *Phys. Lett.* A **380** 3302
[34] Bersuker I B 2010 *Electronic Structure and Properties of Transition Metal Compounds: Introduction to the Theory* (New York: Wiley)
[35] Abdeen A M 1999 *J. Magn. Magn. Mater.* **192** 121
[36] Fritsch D and Ederer C 2012 *Phys. Rev.* B **86** 014406
[37] Ugendar K, Samanta S, Rayaprol S, Siruguri V, Markandeyulu G and Nanda B R K 2017 *Phys. Rev.* B **96** 035138
[38] Idrissi L, Tahiri N, El Bounagui O and Ez-Zahraouy H 2020 *J. Supercond. Nov. Magn.* **33** 1369
[39] Panwar K, Tiwari S, Bapna K, Kumar K, Heda N L, Phase D M and Ahuja B L 2020 *J. Alloys Compd.* 154835
[40] Tamerd M A, Abraime B, Lahmar A, El Marssi M, Hamedoun M, Benyoussef A and El Kenz A 2020 *Superlattices Microstruct.* **139** 106401
[41] Khan M A, Kashyap A, Solanki A K, Nautiyal T and Auluck S 1993 *Phys. Rev.* B **48** 16974
[42] Tributsch H 1977 *Z. Für Naturforschung* A **32** 972
[43] Dileep K, Loukya B, Pachauri N, Gupta A and Datta R 2014 *J. Appl. Phys.* **116** 103505
[44] Shan W, Walukiewicz W, Ager J W III , Haller E E, Geisz J F, Friedman D J, Olson J M and Kurtz S R 1999 *Phys. Rev. Lett.* **82** 1221
[45] Penn D R 1962 *Phys. Rev.* **128** 2093
[46] Khoshman J M, Jakkala P, Ingram D C and Kordesch M E 2016 *J. Non-Cryst. Solids* **440** 31
[47] Ambrosch-Draxl C and Sofo J O 2006 *Comput. Phys. Commun.* **175** 1